CONFERENCE PRE-PRINT

EFFECT OF ELECTRON CYCLOTRON WAVES ON PLASMA WITH RUNAWAY ELECTRONS

Pavel Aleynikov
Max-Planck-Institut für Plasmaphysik
Greifswald, Germany
Email: pavel.aleynikov@ipp.mpg.de

Alexander Battey
EPFL
Lausanne, Switzerland

Carlos Paz-Soldan
Columbia University
New York, USA

Eric Hollmann
UC San Diego
La Jolla, CA, USA

Andrey Lvovskiy
General Atomics
San Diego, USA

Claudio Marini
UC San Diego
La Jolla, CA, USA

Daisuke Shiraki
Oak Ridge National Lab
Oak Ridge, TN, USA

Charles Lasnier
Lawrence Livermore National Lab
Livermore, CA, USA

Abstract

Runaway electrons generated during tokamak disruptions are a major concern for the safe operation of future tokamaks. Interaction of runaway electrons with waves is one of the potential mechanisms for their mitigation. The study investigates the effect of electron-cyclotron (EC) waves on post-disruption plasma with runaway electrons. ”Free space” O- and X-mode EC waves are routinely used for plasma heating (ECH) and current drive. However, these modes do not interact directly with relativistic electrons and cannot be injected into plasma with a density above the corresponding cutoff density. In contrast, the internal slow X-mode is capable of resonant interaction with runaway electrons. The paper reports on experiments conducted on the DIII-D tokamak, where the internal slow X-mode was generated via the so-called OX (Ordinary-to eXtraordinary) mode conversion, a process previously explored in space plasmas to understand planetary radio emissions, auroral kilometric radiation, and particle acceleration. The OX process has also been considered for heating and current drive in overdense plasmas of tokamaks and stellarators. In this experiment, the application of ECH during the runaway electron plateau resulted in a significant increase in background plasma density, along with a doubling of the loop voltage and runaway electron synchrotron emission. These observations indicate effective mitigation of the runaway electron beam. It is noteworthy that when pre-calculated OXB conditions are met, a characteristic density spike forms on the density profile. Modeling suggest that collisional dynamics play a significant role in the observed effects. The modeling indicates that a further increase in background density and temperature is prevented by strong line emission resulting from high argon (Ar) concentration.

1. INTRODUCTION

Runaway electrons (REs) generated during major tokamak disruptions pose a critical risk for next-step devices, where large machine size and high current amplify the potential for wall damage [1, 2]. Wave–particle interactions offer a non-invasive handle on RE dynamics by modifying pitch and energy through resonant processes, complementing collisional [3] and MHD-based mitigation strategies [4]. Among radio-frequency actuators, electron-cyclotron (EC) systems are particularly attractive due to their precise geometry control and mature technology for heating and current drive in conventional regimes. However, the post-disruption plasma is often overdense with respect to the injected frequency, and "free-space" O- and X-modes are reflected at relatively low cutoffs, limiting direct EC access when RE control is most needed. Positive effect of Electron Cyclotron Heating (ECH) on RE in pre-disruption conditions have been observed in tokamaks [5].

A promising path to overcome cutoff limitations is mode conversion at the O-mode cutoff, whereby an externally launched O-mode couples to the internal slow-X (sX) branch; in some conditions the wave may subsequently convert to an electron-Bernstein (B) mode (the OXB pathway) [6]. Unlike free-space O- an X-mode, the sX branch exists behind the O-mode cutoff and can propagate in overdense plasmas. Crucially, for highly relativistic electrons with Lorentz factor $\gamma \gg 1$ the cyclotron resonance condition implies that efficient interaction at wave frequency close to cyclotron frequency, $\omega \sim \omega_{ce}$, requires order-unity parallel refractive index $N_\parallel$. This criterion is compatible with sX rays refracting toward $N_\parallel \sim 1$. Thus, sX offers a route to bring high-frequency power into the overdense post-disruption plasma and to couple it resonantly to REs.

Realizing this scenario experimentally imposes two coupled requirements. First, an O-mode cutoff surface must form along the beam path. For DIII-D's 110 GHz system, the corresponding density $n_e \approx 1.5 \times 10^{20}\ \mathrm{m}^{-3}$ is not achieved in standard pre-disruption operation but can arise during the RE plateau formed after argon pellet injection. Second, geometry matters: cold-plasma theory and full-wave calculations predict a narrow conversion window around an optimal $N_\parallel$ (corresponding to an injection cone of only a few degrees) for efficient O-sX coupling [7, 8, 9]. Meeting this window in an evolving post-disruption equilibrium requires pre-calculations of the launcher sightlines and, where necessary, controlled vertical plasma position to bring the conversion window into view.

This work (i) reviews the theoretical background of the O-sX mode conversion in overdense, post-disruption plasmas; (ii) presents ray-tracing and full-wave modeling that predict the conversion efficiency under relevant conditions; (iii) reports DIII-D experiments implementing this scheme during runaway-electron plateaus. (iv) The analysis suggests experimental access to the sX branch and an indirect impact on the RE beam through background-plasma modification. Direct, unambiguous evidence of resonant wave–particle interaction was not obtained.

The paper is organized as follows. Section 2 reviews the theoretical background for the physics relevant to relativistic electrons and wave mode conversion. Section 3 describes the experimental setup in the context of O-sX conversion. Section 4 presents observations and analysis, and Section 5 summarizes the implications for runaway-electron control.

2. THEORETICAL BACKGROUND

2.1. RE wave resonances

In a homogeneous plasma, the interaction of relativistic electrons with waves is governed by the cyclotron resonance condition

$$1 - N_\parallel \, \beta \cos\theta \; - \; \frac{n\,\omega_{ce}}{\gamma\,\omega} \; = \; 0, \tag{1}$$

where ω is the wave frequency, $N_\parallel = ck_\parallel/\omega$ is the parallel refractive index, $\beta = v/c$, θ is the electron pitch angle, n is the harmonic number, $\omega_{ce} = eB/m_e$ is the (non-relativistic) electron cyclotron frequency, and γ is the Lorentz factor.

Figure 1 displays all branches of the cold-plasma dispersion relation that are resonant with an electron of $\gamma = 20$ and zero pitch angle. The construction is as follows. For the specified γ and θ, Eq. (1) is used to obtain $N_\parallel(\omega)$ for each frequency. The pair $(\omega, N_\parallel)$ is then inserted into the cold-plasma dispersion relation to solve for the perpendicular refractive index $N_\perp$ on the available branches. We plot the resulting resonant $N_\perp$ for $n = 0$ (Cherenkov resonance) and $n = -1$ (anomalous Doppler resonance). The figure corresponds to the case of plasma frequency ω_p greater than ω_c.

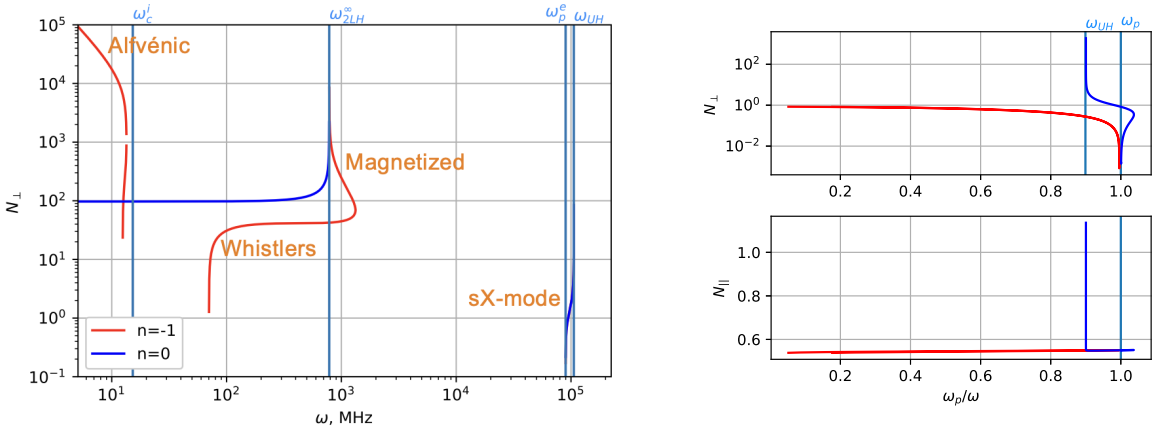

FIG. 1. Left: Cold-plasma waves resonant with a runaway electron ($\gamma = 20$, pitch angle $\theta = 0$) for the $n = 0$ and $n = -1$ when $\omega_p > \omega$. Right: Ray-tracing calculation of the O-sX mode conversion setup in DIII-D. The O-mode propagates (red curve) towards the cutoff $\omega = \omega_p$ and is reflected back in WKB approximation. sX-mode (blue) is generated behind the cutoff.

The low-frequency Alfvén waves and the whistler branches near the lower-hybrid range admit resonances and have indeed been observed in tokamak experiments in the context of runaway electrons [10, 11]. By contrast, although the cold-plasma dispersion supports waves in the upper-hybrid range that satisfy the resonance condition (1) for relativistic electrons, namely the slow-X mode, such high-frequency modes have, to our knowledge, not been reported in the runaway-electron context.

As shown in Fig. 1 the resonant slow-X mode exists in the region of plasma between the upper-hybrid (UH) resonance $\omega_{UH} = \sqrt{\omega_p^2 + \omega_c^2}$ and the O-mode cut-off $\omega = \omega_p$. These waves can enter or escape the plasma either from the high-field-side (HFS), provided that the trajectory does not cross the UH resonance, or via a so-called O-sX conversion process from the low-field side (LFS). The HFS access is typically limited in tokamaks. DIII-D tokamak is equipped with gyrotrons capable of injection the waves with relevant frequencies from the LFS. In the next section we therefore consider the possibility of generating the slow-X mode via the OX conversion process in a setting of DIII-D tokamak.

2.2. O-mode to sX-mode conversion

"Free space" O- and X-mode EC waves are routinely used for plasma heating and current drive. However, these modes do not interact directly with relativistic electrons and cannot be injected into plasma with a density above the corresponding cutoff density. In contrast, the internal sX-mode is capable of resonant interaction with runaway electrons as shown in the previous section. A unique opportunity exist to excite the sX-mode via the so-calles on O-sX mode conversion process.

From the cold plasma dispertion relation it follows that the O and sX branches coalesce at the plasma frequency, $\omega = \omega_p$, when the parallel refractive index satisfies

$$N_\parallel^2 \;=\; 1 - \frac{\omega_p^2}{\omega(\omega + \omega_c)}.$$

This condition defines an optimal value of $N_\parallel^{\rm opt} \approx 0.58$ for the second harmonic heating, $\omega \approx 2\omega_c$, corresponding to an injection angle of approximately 55° to $\mathbf{B}$.

To realize O-sX conversion experimentally, the launch geometry must match the plasma configuration. In DIII-D setting it means that the ECRH launching angles have to be set based on the equilibrium and density profile data. Figure 1 (right) shows a ray-tracing calculation for an optimal scenario for a relevant plasma configuration in DIII-D. The equilibrium is obtained from the efit reconstruction of the shot #194982 at the runaway plateau phase at t = 500 ms. The launchers positions in DIII-D have cylindrical coordinates R = 2.397 m and Z = 0.678 m. The density profile is chosen arbitrarily for this demonstration. The O-mode propagates up to the corresponding

cut-off where it is converted to the slow-X mode, which at first propagates a little further into the plasma but then turns around and approaches the UH resonance. As it approaches the UH resonance the parallel reflective index increases and eventually exceeds unity. At this stage the slow-X mode can interact resonantly with relativistic electrons as explained in the previous Section. Note in the cold plasma limit the sX mode propagation stops at the UH resonance, however when finite plasma temperature is taken into account the sX-mode continues it's trajectory into the plasma as the Berstein wave. This is not considered here.

2.3. Full wave calculation of conversion efficiently

In WKB approximation the conversion efficiency is expected to be 100% for the optimal $N_{\|}$, but degrades exponentially for the non-optimal injections [7, 12].

Figure 2 (left) presents a snapshot from the full-wave simulation of O-sX conversion using the 3D full-wave code CUWA [9]. An O-mode beam is launched from the vacuum side (bottom boundary) and propagates to its cutoff layer, where a small fraction is reflected. Beyond the cutoff, an sX wave is generated; it propagates some distance into the plasma, refracts, turns, and then travels back toward the launcher. Upon approaching the UH resonance the wavelength shortens rapidly; in the present model this leads to strong numerical damping of sub-grid scales, so the wave amplitude vanishes at the UH layer. In this regime the conversion fraction is inferred from boundary Poynting fluxes at the injection, $P_{O,\mathrm{inc}}$, and the reflectio $P_{O,\mathrm{ref}}$ areas. The effective fraction retained in the plasma in then $T_{\mathrm{eff}} = 1 - P_{O,\mathrm{inc}}/P_{O,\mathrm{ref}}$. Figure 2 (right) shows the results of the conversion efficiency

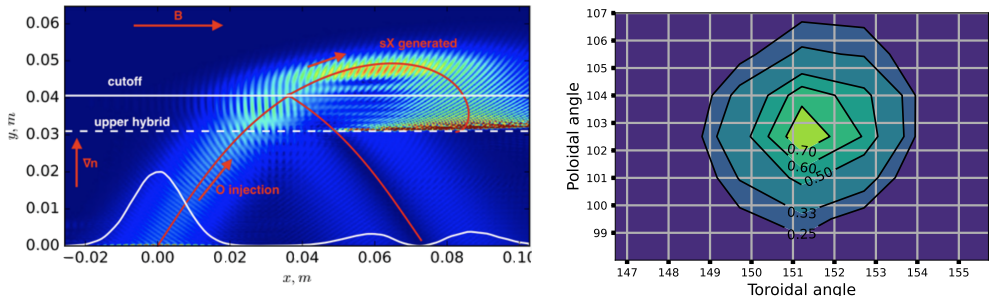

FIG. 2. Left: Snapshot of the wave electric field calculation of an O-sX conversion process (color-coded), ray tracing (solid red). The antenna is located in the bottom left corner. The O-mode cutoff and Upper Hybrid resonance layers are indicated with white lines. Right: 3D full-wave calculation of the O-sX conversion fraction in DIII-D post disruption plasma.

calculations scan over the injection angles. These calculations take realistic beam shape, launching parameters and plasma curvature of DIII-D into account. The predicted window width (with ¿50% conversion) is only a few degrees, underscoring the sensitivity of O-sX coupling to the injection geometry. The maximum expected conversion is around 75%.

2.4. Expected effect on plasma and RE

Realizing O-sX conversion in experiment first requires that an O-mode cutoff exist somewhere along the beam path. For the DIII-D ECH system operating at $f = 110$ GHz, the cutoff density is $n_c \approx 1.5 \times 10^{20}$ m^{-3}, which is not attainable in standard (pre-disruption) tokamak scenarios. In this work, however, the EC wave is injected into a runaway-electron plateau formed by argon injection (triggering a thermal quench followed by a current quench). During the plateau one can admix substantial neutral gas, yet experiments indicate that the ionized density remains relatively low; thus, the plasma is underdense with respect to 110 GHz and contains no O-cutoff surface. Consequently, immediate O-sX conversion is not expected at injection, and the megawatt-level EC power initially interacts only weakly with the backgound plasma.

In the absence of an O-mode cutoff, the launched O-mode traverses the cold companion plasma ($T_e \sim 1$ eV), and the dominant dissipation is non-resonant collisional damping [13]. The corresponding absorption length is $L_P \simeq \frac{c}{\nu_e}$, , where ν_e is the collisional freqency. The resulting L_P is up to a meter-scale, providing a modest but finite power deposition even in initially underdense conditions. As ionization proceeds and the local density rises toward the cutoff, EC power deposition concentrates in a narrow layer near the UH. As the electron density

locally rises to the O-mode cutoff for 110 GHz, an O-sX conversion layer forms and the power flow bifurcates: some fraction of the O-mode is reflected, whereas the converted sX refracts and turns toward the upper-hybrid (UH) resonance. Because the group velocity of sX collapses near the UH layer, the wave energy piles up and is strongly attenuated collisionally, producing a narrow, localized heat source in place of the initially broad volumetric absorption. Formation of such a non-monotonic density and temperature profiles are thus expected to be one of the main manifistation of the successful o-sX mode conversion.

This localization is expected to evolve in time. The combined effect of increasing density (advecting the O-cutoff and the conversion layer inward) and rising temperature (reducing the electron–ion collision frequency, $\nu_{ei} \propto n_e T_e^{-3/2}$) lessens collisional damping and allows the sX wave to survive over longer path lengths. In other words, the deposition region can progressively migrate as the plasma warms and ionizes—effectively opening a propagation corridor for sX deeper into the plasma. Once the mode persists over sufficient distance and time, conditions become favorable for resonant interaction with runaway electrons (via $n = 0$ or $n = -1$ harmonics, depending on the evolving $N_\parallel$), enabling the high-frequency branch to influence the runaway beam dynamics.

3. EXPERIMENTAL SETUP

Experiments were performed on the DIII-D tokamak in intentionally disrupted discharges designed to form a post-disruption runaway-electron (RE) plateau using argon pellet injection. The baseline scenario is an inner-wall-limited, low-elongation plasma at relatively low pre-disruption density, with electron cyclotron heating (ECH) used to condition the target prior to the disruption trigger. Typical pre-disruption plasma parameters in this work are $I_p \simeq 0.7$ MA, $B_T \simeq 2.0$ T, and line-averaged density $\langle n_e \rangle \sim 10^{19}$ m^{-3}, with ECH power in MW range. Following conventional RE-production practice on DIII-D, a cryogenic Ar pellet is injected from the low-field-side (LFS) mid-plane to initiate a fast shutdown, it triggers the thermal quench (TQ) and current quench (CQ), establishing an RE plateau. The Massive Gas Injection (MGI) system is then used to admix Helium gas such that it is possible to reach high densities after ECH ionisation. The ECH system, operated at $f = 110$ GHz, launches from the LFS. Due to safety reasons the maximum allowed ECH pulse length was 250 ms (and 500 ms in later experiments).

In the standard mid-plane–centered equilibrium (magnetic axis near $Z \approx 0$), the optimal O→sX conversion cone lies outside the mechanical steering envelope of the LFS ECRH launchers. To place the local $N_\parallel$ at the O-cutoff within the predicted narrow window, we instead manipulate the plasma geometry: a controlled upward shift of the plasma column increases the poloidal incidence of the pre-set beams and brings the cutoff surface into the launcher line of sight. This geometric adjustment moves the conversion window into the accessible angular range without changing ECH settings. This is the basis for the vertical position scans used in our experiments.

4. EXPERIMENTAL OBSERVATIONS

In shot #194984 the plasma position was pre-programmed to scan the O→sX conversion geometry during a single EC pulse: three gyrotrons were preset to fixed steering angles, energized for 250 ms, while the plasma vertical position was ramped to sweep the local $N_\parallel$ at the anticipated O-cutoff location through the predicted conversion window. Figure 3 shows the evolution of the plasma vertical position (left) and the evolution of the optimal injection angles calculated for the sequence of equilibrium reconstructed with efit after the experiment (right). The launching angles pre-set for this experiment are indicated with the black circle ($\theta = 104°$, $\phi = 151°$). The plasma approaches optimal configuration after $t = 700$ ms. The ECH is applied between $t = 600$ ms and $t = 850$ ms.

As the configuration evolved away from the initially non-optimal geometry, the Thomson scattering (TS) vertical chord recorded a low, broadly distributed electron-density profile (bottom panel between $t = 600$ ms and $t = 700$ ms in Fig. 4). Note that the vertical axis in the bottom panel of Fig. 4 indicates Z coordinate of the TS viewpoints (also shown with red dots in Fig. 3). During the vertical sweep, when the computed conversion fraction increases (black curve in the bottom panel of Fig. 4) at $t = 700$ ms, the TS signal changed character: a narrow, edge-localized density spike emerged near $Z \approx 0.65$ m. The appearance of this spike coincident with the approach to the conversion window is consistent with formation of an O-cutoff layer and efficient O-sX coupling, replacing the initially broad collisional absorption by a localized source near the conversion/UH region.

At the same time, the loop voltage required by the feedback system to sustain I_p rises sharply (middle panel of Fig. 4), indicating an increase in the effective resistivity of the RE-dominated current channel. This rise starts

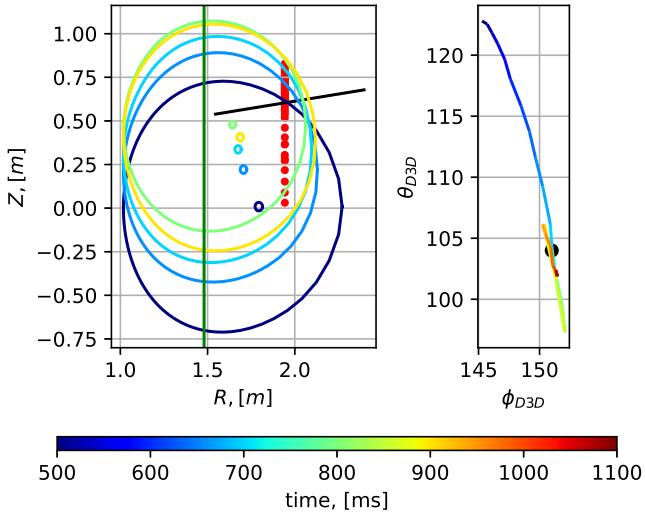

FIG. 3. Efit reconstruction of the evolution of plasma position in #194984 (left) and corresponding optimal ECH injection angles (right).

at the begining of ECH application but is most pronounced with the approach to the O-sX conversion. In the same interval, both the visible synchrotron intensity and the scintillator hard-X-ray (HXR) signal increase markedly.

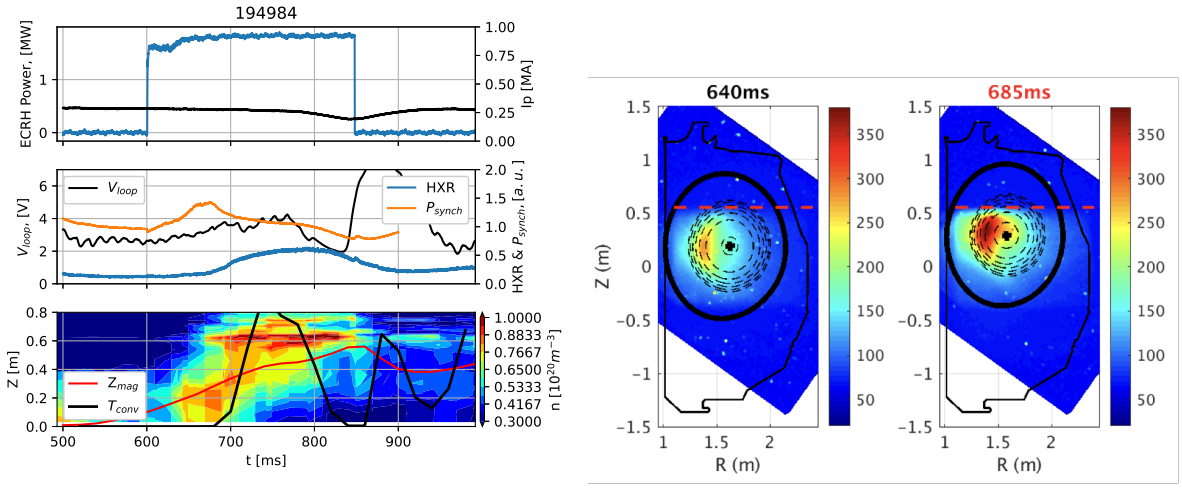

FIG. 4. Left: Time-traces of shot #194984. ECH power and plasma current (top); loop voltage, HXR scintillator "bgo330p", visible synchrotron signal (middle); Thomson scattering (color-coded), magnetic axis position, calculated OX conversion fraction (bottom). Right: Visible-camera snapshots of synchrotron emission from the RE beam.

On the middle panel of Fig. 4, the synchrotron trace (orange) first rises, then plateaus, and eventually decreases. This trend is diagnostic-geometric, not physical weakening of the RE emission: the plotted curve is the field-of-view (FOV) -integrated brightness from the tangential camera, whereas during the vertical sweep the RE beam centroid gradually moves out of the camera FOV. As a result, the total signal saturates and falls even though the local emissivity continues to increase. Indeed, the peak pixel intensity within the visible portion of the beam keeps rising and nearly doubles, as evidenced by the two camera snapshots in Fig. 4 (right).

An important observation is that the TS-derived density profile is not up–down symmetric about the magnetic axis. As shown in the bottom panel of Fig. 4, a pronounced maximum appears at $Z \approx +0.6$ (in machine coordinates), while only a modest increase is seen at the location symmetric below the magnetic axis (marked by the red line). This indicates that the EC-driven heating and ionization is insufficient to warm an entire flux surface

uniformly under these conditions. Instead, the measurements suggest a three-dimensional deposition structure: density and temperature are toroidally and poloidally localized near the ECH launcher line of sight, with values decreasing along the connected field line and more steeply across it. Note that in this experiment the TS does not measure local densities above the O-mode cut-off of $1.5 \cdot 10^{20} m^{-3}$ - the density required for O-sX conversion.

Figure 5 shows the time traces of the experiment #199766. In this experiment the equilibrium was held fixed at optimal position. The black curves in the lower panel shows the computed O-sX conversion efficiency for two gyrotron groups. During this experiment the TS system observes the formation of a more flux-surface–uniform annulus of enhanced electron density. Local TS points reach—and in places exceed — the O-mode cutoff for 110 GHz, $n_c \approx 1.5 \times 10^{20}$ m^{-3}. The densities of $n_e \approx 1.75 \times 10^{20}$ m^{-3} are recorded. Consistently, the middle panel (CO_2 interferometer) shows the line-integrated density rising above the n_c during periods of effective conversion.

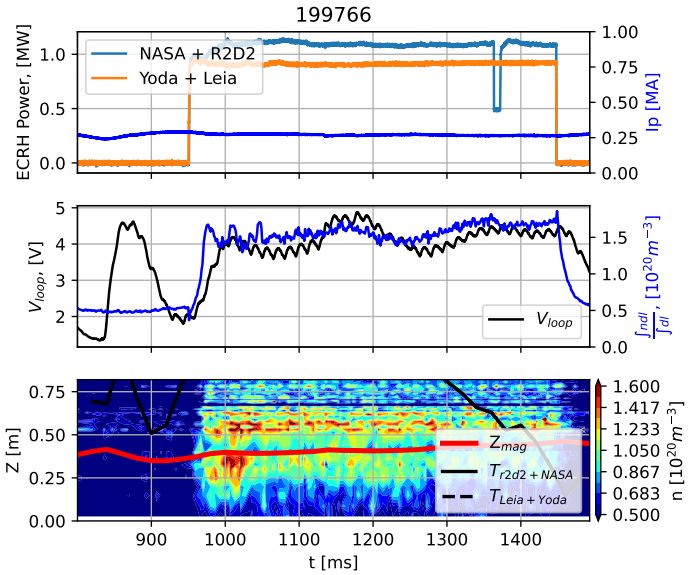

FIG. 5. Same as in Fig. 4 for #199766. In the middle panel the line integrated density (divided over the path length obtained from efit reconstruction) is shown.

5. SUMMARY

Efficient O-sX conversion requires careful control of the plasma configuration and the O-mode launch parameters. We have developed a scheme that allows O-sX conversion in the post-disruption runaway plateau regime on the DIII-D tokamak. The application of ECH during the runaway electron plateau resulted in a significant increase of the background plasma density (apparently exceeding the cutoff density), together with a doubling of the loop voltage and of the runaway electron synchrotron emission. These observations indicate an effective mitigation of the runaway electron beam. The effect is more pronounced when the pre-calculated O-sX conditions are met, a characteristic density spike forms on the density profile in this case. Kinetic modeling and 1D impurity and neutral transport modeling suggest that collisional dynamics play a significant role in the observed effects. Heating of the ambient plasma increases the ionisation level of the argon impurities and their local concentration, making runaway scattering more efficient. This effect appears to overwhelm the resonant interaction. Although we observed a pronounced effect of the ECH on post-disruption runaway plateau, we did not register any direct evidence of a resonant wave-particle interaction (the indirect effects due to background modification appear to overwhelm it). Nonetheless, our study highlights the potential of ECH/O-sX heating as a novel approach to control runaway electrons via one of the two mechanisms: heating of the background plasma or resonant wave-particle interaction.

ACKNOWLEDGEMENTS

This material is based upon work supported by the U.S. Department of Energy, Office of Science, Office of Fusion Energy Sciences, using the DIII-D National Fusion Facility, a DOE Office of Science user facility, under Award(s) DE-FC02-04ER54698, DE-SC0021622 (Frontiers), DE-SC0022270 (CU), and DE-FG02-07ER54917

(UCSD). This work was supported by the US Department of Energy Office of Fusion Energy Sciences at Lawrence Livermore National Laboratory (LLNL) under contract No. DE-AC52-07NA27344. This work was supported by the US Department of Energy Office of Fusion Energy Sciences at Oak Ridge National Laboratory (ORNL) under contract No. DE-AC05-00OR22725.

REFERENCES

[1] S. Ratynskaia et al. "Runaway electron-induced plasma facing component damage in tokamaks". In: (2025). arXiv: 2506.10411 [physics.plasm-ph].

[2] R.A. Pitts et al. "Plasma-wall interaction impact of the ITER re-baseline". In: *Nuclear Materials and Energy* 42 (2025), p. 101854. ISSN: 2352-1791. DOI: https://doi.org/10.1016/j.nme.2024.101854.

[3] Michael Lehnen et al. "Disruptions in ITER and strategies for their control and mitigation". In: *Journal of Nuclear materials* 463 (2015), pp. 39–48.

[4] Carlos Paz-Soldan et al. "A novel path to runaway electron mitigation via deuterium injection and current-driven MHD instability". In: *Nuclear Fusion* 61.11 (2021), p. 116058.

[5] J Decker et al. "Expulsion of runaway electrons using ECRH in the TCV tokamak". In: *Nuclear Fusion* 64.10 (2024), p. 106027.

[6] HP Laqua et al. "Resonant and nonresonant electron cyclotron heating at densities above the plasma cutoff by OXB mode conversion at the W7-AS stellarator". In: *Physical review letters* 78.18 (1997), p. 3467.

[7] J. Preinhaelter and V. Kopecký. "Penetration of high-frequency waves into a weakly inhomogeneous magnetized plasma at oblique incidence and their transformation to Bernstein modes". In: *Journal of Plasma Physics* 10.1 (1973). Cited by: 202, pp. 1–12. DOI: 10.1017/S0022377800007649.

[8] A G Shalashov and E D Gospodchikov. "On O–X mode conversion near the cut-off surfaces in 3D sheared magnetic field". In: *Plasma Physics and Controlled Fusion* 52.11 (Sept. 2010), p. 115001. DOI: 10.1088/0741-3335/52/11/115001.

[9] Pavel Aleynikov and Nikolai B Marushchenko. "3D Full-Wave modelling and EC mode conversion in realistic plasmas". In: *EPJ Web of Conferences*. Vol. 203. EDP Sciences. 2019, p. 01003.

[10] Donald A Spong et al. "First direct observation of runaway-electron-driven whistler waves in tokamaks". In: *Physical Review Letters* 120.15 (2018), p. 155002.

[11] A Lvovskiy et al. "Parametric study of Alfvénic instabilities driven by runaway electrons during the current quench in DIII-D". In: *Nuclear Fusion* 63.4 (2023), p. 046011.

[12] E Mjølhus. "Coupling to Z mode near critical angle". In: *Journal of plasma physics* 31.1 (1984), pp. 7–28.

[13] Pavel Aleynikov and Boris Breizman. "Stability analysis of runaway-driven waves in a tokamak". In: *Nuclear Fusion* 55.4 (2015), p. 043014.